THE JOURNAL OF PHYSICAL CHEMISTRY C
A JOURNAL OF THE AMERICAN CHEMICAL SOCIETY

pubs.acs.org/JPCC

Article

Atypical Magnetic Behavior in the Incommensurate $(CH_3NH_3)[Ni(HCOO)_3]$ Hybrid Perovskite

Breogán Pato-Doldán,[⊥] Laura Cañadillas-Delgado,[⊥] L. Claudia Gómez-Aguirre, M. A. Señarís-Rodríguez, Manuel Sánchez-Andújar, Óscar Fabelo,* and Jorge Mira*

Cite This: *J. Phys. Chem. C* 2023, 127, 3330−3338

Read Online

ACCESS | Metrics & More | Article Recommendations

ABSTRACT: A plethora of temperature-induced phase transitions have been observed in $(CH_3NH_3)[M(HCOO)_3]$ compounds, where M is Co(II) or Ni(II). Among them, the nickel compound exhibits a combination of magnetic and nuclear incommensurability below Néel temperature. Despite the fact that the zero-field behavior has been previously addressed, here we study in depth the macroscopic magnetic behavior of this compound to unveil the origin of the atypical magnetic response found in it and in its parent family of formate perovskites. In particular, they show a puzzling magnetization reversal in the curves measured starting from low temperatures, after cooling under zero field. The first atypical phenomenon is the impossibility of reaching zero magnetization, even by nullifying the applied external field and even compensating it for the influence of the Earth's magnetic field. Relatively large magnetic fields are needed to switch the magnetization from negative to positive values or vice versa, which is compatible with a soft ferromagnetic system. The atypical path found in its first magnetization curve and hysteresis loop at low temperatures is the most noticeable feature. The magnetization curve switches from more than 1200 Oe from the first magnetization loop to the subsequent magnetization loops. A feature that cannot be explained using a model based on unbalanced pair of domains. As a result, we decipher this behavior in light of the incommensurate structure of this material. We propose, in particular, that the applied magnetic field induces a magnetic phase transition from a magnetically incommensurate structure to a magnetically modulated collinear structure.

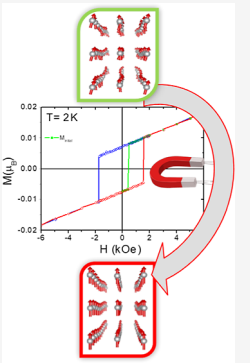

INTRODUCTION

Coordination polymers are hybrid inorganic/organic structures formed by metal cation centers that are linked by ligands in the form of one-, two-, or three-dimensional crystalline structures. Such ligands open spaces in the structure with the capacity of hosting diverse cations. This allows a tailoring that has yielded a plethora of potential applications and functionalities,[1,2] thanks to their optical,[3] ferroelectric,[4−6] or magnetic properties.[7,8]

These materials are of the formula $(amineH)[M(HCOO)_3]$ (where M is a divalent transition-metal cation) which presents an ABX_3 perovskite structure, where the metal cations (B = M^{2+}) linked by formate groups (X = $HCOO^-$) form the BX_3 skeleton and protonated amine cations (amineH) occupy the cavities (A = $[CH_3NH_3]^+$, $[(CH_3)_2NH_2]^+$, $[CH_3CH_2NH_3]^+$, $[(CH_2)_3NH_2]^+$, $[C(NH_2)_3]^+$, $[HONH_3]^+$, $[NH_2NH_3]^+$, etc.).[9−12] Some of their magnetic, dielectric, and even multiferroic properties have already been described.[13,14] The formate anion linker is a good choice for several reasons: it is a short ligand, and it can adopt various bridging modes and extended structures, thus providing significant magnetic coupling between magnetic metal sites.[15]

Typically, the $(amineH)[M(HCOO)_3]$ compounds display weak ferromagnetic arrangements in the range of 8−36 K depending on the specific metal.[16,17] This feature can be explained by the presence of a noncentrosymmetric ligand (formate) between the magnetic ions, which allows the occurrence of Dzyaloshinsky−Moriya (DM) interactions (antisymmetric exchange), giving rise to spin canting.[18−20]

When a methylammonium cation is placed inside the cuboctahedral cavities, the resulting $(CH_3NH_3)[M(HCOO)_3]$ materials show weak ferromagnetic ordering below T_N.[21−24] Within this family, $(CH_3NH_3)[Ni(HCOO)_3]$ is especially appealing, as it displays negative susceptibility in some zero-field-cooled (ZFC) magnetization versus temperature curves.[21]

When a magnetic material is under the influence of an external magnetic field, its global magnetic moment tends to align, usually, with the external field. However, in some cases, the alignment of the net magnetization occurs in the opposite direction of the magnetic field (negative magnetization). This behavior has been known since long ago in some ferrimagnets below their compensation temperature.[25] Among them, several families of coordination polymers show negative magnet-

Received: November 29, 2022
Revised: January 10, 2023
Published: February 2, 2023

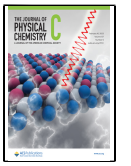

ization, for example, formates,[26,27] oxalates,[28−30] and Prussian blue analogues.[31−36]

In all these cases, the effect can be explained by the existence of two different subnets with different net magnetizations and ordering temperatures. The first subnet forces the second one, due to the antiferromagnetic exchange, to order toward the opposite direction of the applied magnetic field.

Negative magnetization curves have also been observed in weak ferromagnetic systems like $LaVO_3$ or YVO_3.[37−39] The mechanism could also be the same in the case of negative ZFC magnetization observed at low fields in Fe_2OBO_3,[40] but it has also been suggested as an explanation for the competition between inter-ribbon versus intraribbon exchange interactions of different signs (and temperature dependences), like in the case of Co_2VO_4 ($Co^{2+}[Co^{2+}V^{4+}]O_4$), arguing that the competition between Co^{2+}−O−V^{4+} and direct V^{4+}−V^{4+} cants the vanadium and cobalt spins in opposite directions, leading to a compensation point and magnetization reversal.[41]

Nevertheless, in $(CH_3NH_3)[Ni(HCOO)_3]$, the mechanism of negative magnetization and the anomalies observed in the hysteresis loops cannot be explained using a noncompensation model between magnetic subnets.

The case of this compound is quite uncommon, and it needs specific circumstances to show up. Cañadillas-Delgado et al. have recently analyzed it by neutron diffraction[42] and found that this material is a rare case, where structural incommensurability and magnetic incommensurability both have a proper character. In the following sections, its magnetic behavior is deeply analyzed using magnetometry measurements to confirm the proper character of the magnetic incommensurability and to unveil the reasons for its rare magnetic behavior, which could also help explain similar features in other parent coordination polymers with a perovskite structure.

METHODS

Materials. $NiCl_2$ (98%, Aldrich), methylamine hydrochloride (99% Aldrich), sodium formate (≥99%, Aldrich), and *N*-methylformamide (99%, Aldrich) were commercially available and used as purchased without further purification.

Synthesis. A mixture of $NiCl_2$ (1 mmol), NaCHOO (3 mmol), CH_3NH_2·HCl (1 mmol), methylformamide (8 mL), and H_2O (8 mL) was heated in a Teflon-lined autoclave (45 mL) at 140 °C for 3 days. After slow cooling to room temperature, green crystals suitable for single-crystal X-ray crystallographic analysis were obtained. They were collected, washed with ethanol, and dried at room temperature. Large single crystals, suitable to carry out magnetic measurements, were obtained by slowly evaporating the mother liquid for about 4 months at room temperature.

Heat Capacity. Heat capacity as a function of temperature was measured on a single crystal using a Quantum Design PPMS (physical property measurement system) in the temperature range 1.9−300 K. The sample was fixed to the sample holder with Apiezon N grease.

Measurement of Magnetic Properties. Magnetic properties were studied in a Quantum Design MPMS superconducting quantum interference device (SQUID) magnetometer in both polycrystalline samples and oriented single crystals. Single crystals were oriented on the X-ray diffraction unit of the University of Santiago de Compostela and mounted on a straw; an error of ±5° along different orientations could occur. ZFC and field-cooled (FC) magnetic susceptibility data were obtained under different magnetic fields in the temperature range $2 \leq T\ (K) \leq 300$. Hysteresis loops in ZFC conditions were obtained at 2 K varying the field up to ±50 kOe. The data were corrected using Pascal's constants to calculate the diamagnetic susceptibility, and an experimental correction for the sample holder was applied. In order to reduce the remnant field in the magnet of the magnetometer, the "reset field" option of the system was used before lowering the temperature for a ZFC curve. Also, in order to test the influence of the remanent field of the magnet (even after resetting of the field), the ultralow field option has been used in some specific measurements, which nulls the applied magnetic field at the specific position of the sample in the chamber. For this, the residual field was measured with a fluxgate magnetometer and then a compensating field was applied in the superconducting solenoid to null the residual one. Even after this operation, a field closer to 0 Oe than −0.1 Oe could not be ensured in all the relevant parts of the chamber.

RESULTS

Crystal and Magnetic Structures. Although the description of the crystal and magnetic structures of $(CH_3NH_3)[Ni(COOH)_3]$ is not the main objective of this work, to better understand the magnetic behavior of this compound, a brief description of the nuclear and magnetic structures based on the neutron single-crystal diffraction data will be discussed in this section.

$(CH_3NH_3)[Ni(COOH)_3]$ shows a structural phase transition at 84 K (see Figure 1 for an overview of the phases of this system), involving a transformation from *Pnma* space group to the incommensurate *Pnma* $(00\gamma)0s0$ space group with wave vector $\mathbf{q} = 0.1426(2)c^*$. The average structure, described in the *Pnma* space group, is distorted by the application of a modulation function that exhibits a sinusoidal behavior. The amplitudes of the displacive modulation are mainly applied over the *b* axis with a small component in the *a* and *c* axes for some atoms.

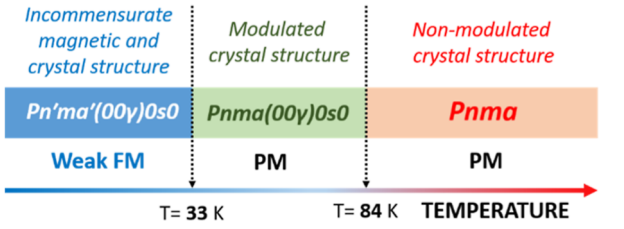

Figure 1. Summary of the phase transitions with temperature in $(CH_3NH_3)[Ni(HCOO)_3]$: from paramagnetism to weak ferromagnetism at 33 K and from an incommensurate to a nonmodulated crystal structure at 84 K.

The application of these modulations induces distortions in the framework and counterions. However, the local structure is not strongly affected. In the case of the NiO_6 octahedron, these distortions produce a displacement of the Ni atom along the *b* axis of ca. 0.3 Å; however, the local environment remains octahedral with values of Ni−O distances between 2.054(2) and 2.076(2) Å.

There is a significant change in the hydrogen-bonded network between the nonmodulated and the modulated phases. The hydrogen atoms of the CH_3 group do not establish any hydrogen bond, neither in the nonmodulated nor in the incommensurate phases. However, two of the three

https://doi.org/10.1021/acs.jpcc.2c08364
J. Phys. Chem. C 2023, 127, 3330−3338

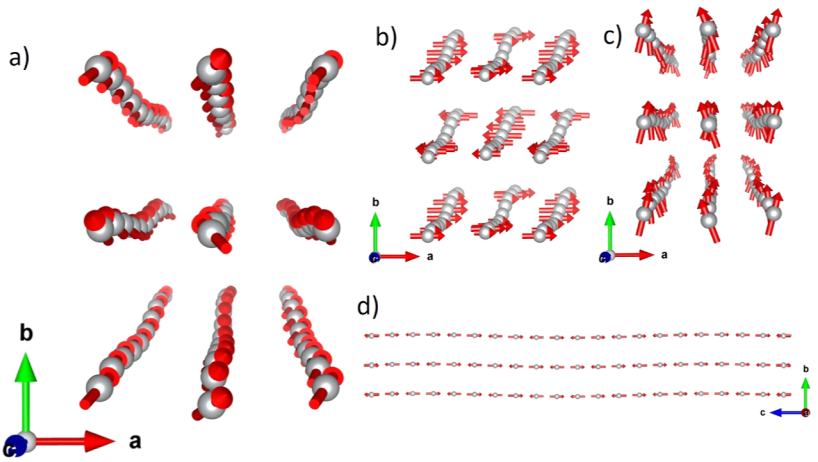

Figure 2. (a) Magnetic structure at 5 K and zero field of $(CH_3NH_3)[Ni(COOH)_3]$. (b) Magnetic moment component along the *a* axis (red), showing that along this direction the system is AF. (c) Magnetic moment component along the *b* axis (green), where there is a global weak ferromagnetic component. (d) Component of the magnetic moments along the *c* axis (blue) that corresponds with the main component and presents a global AF behavior. The magnetic moment amplitudes for the components along the *a* and *b* axes have been multiplied by two for the sake of clarity. The structure represented in (a) is the sum of (b−d).

hydrogen atoms of the NH_3 group clearly set hydrogen bonds with the nearest oxygen atoms of two formate groups, in both phases. However, in the incommensurate phase, the third hydrogen atom of the NH_3 group fluctuates following a sinusoidal distortion between two oxygen atoms from the same formate ligand; this interaction is the most probable origin of the structural modulation.

The combination of displacive and magnetic modes is needed to fit the experimental data. The determination of the compatible superspace magnetic groups has been done by combining two independent modulation vectors, $\mathbf{q} = 0.1426c^*$, which accounts for the structural distortions, and $\mathbf{k} = (0, 0, 0)$, over the previously distorted structure, and therefore are incommensurate from the structural point of view.

The symmetry analysis reveals that below 33 K, $(CH_3NH_3)[Ni(COOH)_3]$ can be described using the $Pn'ma'(00\gamma)0s0$ magnetic superspace group.

This superspace group allows 12 free modes for the magnetic atoms, which are divided into strain, displacive, and magnetic modes. The strain models are considered during the indexing procedure and, therefore, for magnetic analysis, they can be discarded. The second group represents three displacive modes, which are responsible for structural modulation (atomic displacement). The last group involves six pure magnetic modes, three for the *x*, *y*, and *z* components of the homogeneous moment and three sinusoidal modulations with amplitudes along *x*, *y*, and *z*, these last three modes being responsible for proper magnetic contribution.

Below 33 K, the refined model can be described as chains oriented ferromagnetically along the *c* axis and antiferromagnetically coupled with the adjacent along the *a* and *b* directions (C-type antiferromagnet). The magnetic moments are tilted along the *b* axis, giving rise to a nonzero ferromagnetic component along this direction (Figure 2). This contribution arises from the nonzero value of the *y* component of the homogeneous moment and therefore this component has an improper origin. Furthermore, the development of proper incommensurability modes promotes the modulation of the orientation of the magnetic moments, exhibiting a sinusoidal behavior with the main contribution to the magnetic modulation amplitude along the *a* axis. The amplitude of the magnetic modulation along the *b* axis is zero within the experimental error, and the amplitude along the *c* axis is almost 4 times weaker than that along the *a* axis. The effect of these two modulation components produces the nondisplacive modulation of the magnetic moment in the *ac* plane (Figure 2). The contribution of these two components is important for explaining the atypical hysteresis loops, as it will be shown subsequently in the text. The obtained value for the Ni(II) magnetic moment is on average 2.15(7) μ_B; a small modulation in the magnetic moment modulus is observed, although the variation (2.14−2.16 μ_B) is within the error bar of our refinement.

Magnetic Properties. Figure 3 shows the ZFC−FC susceptibility $\chi(T)$ of a polycrystalline sample of $(CH_3NH_3)[Ni(HCOO)_3]$ under an applied field of 1000 Oe, where an increase of the magnetization and divergence of the ZFC−FC curves is visible below $T \approx 33$ K. The most interesting feature is, however, a ZFC curve that shows negative susceptibility until 25 K.

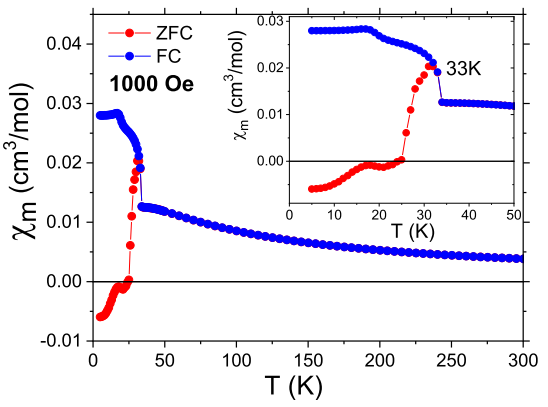

Figure 3. ZFC−FC susceptibility $\chi(T)$ of a polycrystalline sample of $(CH_3NH_3)[Ni(HCOO)_3]$ under an applied field of 1000 Oe.

The linear fit of the susceptibility data above 50 K provides a good agreement to a Curie−Weiss behavior from which the values of $\theta = -65$ K and a $\mu_{eff} = 3.35$ μ_B are calculated (see Table 1).

https://doi.org/10.1021/acs.jpcc.2c08364
J. Phys. Chem. C 2023, 127, 3330−3338

Table 1. Summary of the Results of the Fitting to the Curie–Weiss and Lines Model for a Single Crystal of $(CH_3NH_3)[Ni(HCOO)_3]$ along the Directions [010], [101], and [10−1], Compared against a Polycrystalline Sample Measured at 1000 Oe

		single crystal		
	polycrystalline sample	[010]	[101]	[10−1]
T_{C-W}[a]/K	50−300	68−300	80−300	70−300
R^2 (CW)[b]	0.9998	0.9996	0.9998	0.9995
C/cm^3 kmol^{-1}	1.40	1.13	1.17	1.10
θ/deg	−64.96	−51.6	−53.7	−48.6
$\mu_{eff}/\mu B$	3.35	3.01	3.07	2.97
T_L[c]/K	100−300	100−300	100−300	100−300
R^2 (L)[d]	0.9995	0.9921	0.9999	0.9971
J/cm^{-1}	−9.44	−9.05	−9.47	−10.88
g	2.33	2.15	2.22	2.27

[a]Temperature interval for the fitting to the Curie–Weiss model. [b]Goodness of fit of the Curie–Weiss fitting. [c]Temperature interval for the fitting to the lines model. [d]Goodness of fit of the Lines fitting.

The latter is close to the expected for a Ni^{2+} cation (d^8), with $S = 1$ and $g = 2.00$ ($\mu_{teo} = 2.83\ \mu_B$). The negative value of θ is consistent with a main antiferromagnetic exchange interaction. The apparent negative value of θ could also be due to the single-ion anisotropy expected for Ni^{2+}-coordination compounds, which is not considered in the Curie–Weiss model. Ab initio calculations in the isomorph $(CH_3NH_3)[Co(HCOO)_3]$ compound have determined that the observed weak ferromagnetism commonly attributed to the DM interaction is primarily due to the single-ion anisotropy of Co(II) ions.[23] A similar scenario is expected for the Ni-based compound, where a fit to the Lines model in the temperature range from 100 to 300 K in three different orientations shows a slightly anisotropic behavior of the Landé g-factor (see Table 1).

The magnetic transition at 33 K is also detected in a peak in the thermal dependence of the specific heat at that temperature (Figure 4).

When the ZFC–FC susceptibility $\chi(T)$ is measured in single crystals (along the directions indicated in Figure 5a) for a lower magnetic field (100 Oe), an almost specular behavior between ZFC and FC curves is clearly observed below $T \approx 33$ K, with negative magnetization values more evident than before for the ZFC curve (Figure 5b).

In order to discard any artifact or a possible extrinsic origin of this phenomenon, we examined more in detail our measuring procedures. First, we performed FC magnetization curves under small magnetic fields, that is, magnetization versus temperature curves by cooling the samples under low magnetic fields. We observed then that, when applying a cooling field of −5 or −10 Oe, the ZFC branch of the susceptibility curve measured at 100 Oe (shown in Figure 6) was similar to that in Figure 5b, but, when this cooling field was +5 or +10 Oe, the measured curve at 100 Oe showed an

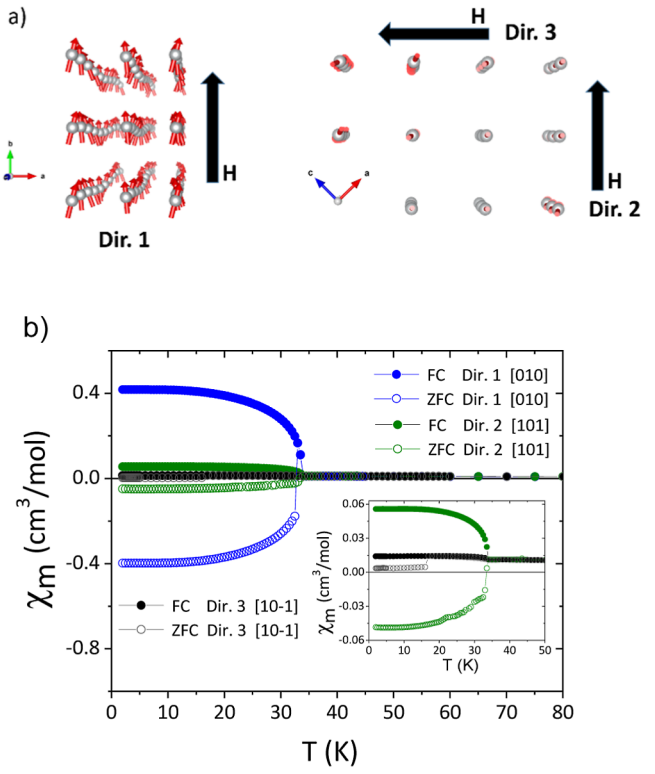

Figure 5. (a) Orientations along where the magnetization has been measured for $(CH_3NH_3)[Ni(HCOO)_3]$. (b) Thermal dependence of χ_m for $(CH_3NH_3)[Ni(HCOO)_3]$ along the orientations [010], [101], and [10−1] and under a field of 100 Oe.

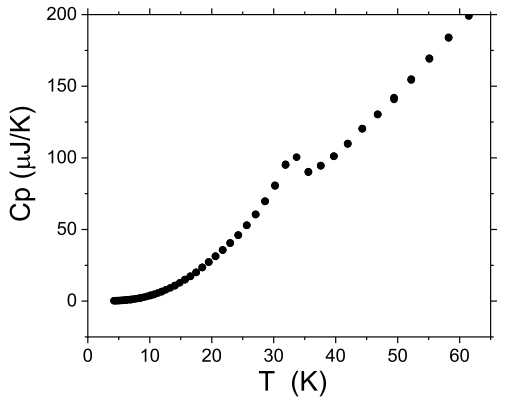

Figure 4. Specific heat capacity (Cp) as a function of the temperature for $[CH_3NH_3][Ni(HCOO)_3]$, where the peak associated with the magnetic transition point is visible.

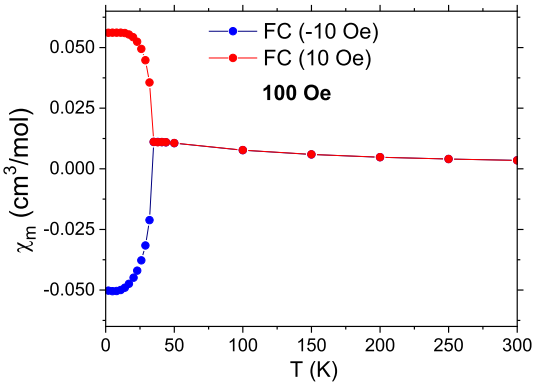

Figure 6. Thermal dependence of χ_m for $(CH_3NH_3)[Ni(HCOO)_3]$ for a polycrystalline sample under a field of 100 Oe, after being FC under +10 and −10 Oe.

https://doi.org/10.1021/acs.jpcc.2c08364
J. Phys. Chem. C 2023, 127, 3330−3338

almost specular behavior; it completely reversed its sign with respect to the previous case.

This means that the system is extremely sensitive to any trapped magnetic field in the magnet: depending on the sign of this trapped field that acts on the sample while cooling, the magnetization defines its sign once the temperature goes below 33 K. This is a crucial point when facing the study of the magnetism of this system; we join the opinion of Belik[43,44] and Kumar and Sundaresan,[45] who have warned about these tricky circumstances in the measurement of the magnetizations of $CoCr_2O_4$ or classical materials in solid-state physics like the perovskites $BiFeO_3$−$BiMnO_3$ and YVO_3.

Actually, even after using the ultralow-field option of our magnetometer to reduce the trapped field acting on the sample chamber, we could not get rid of this problem: fields as low as ±0.1 Oe (which is around one-fifth of the Earth's magnetic field) were enough to completely polarize the magnetization in one direction or the other. Therefore, we conclude that the negative magnetization found after conventional ZFC procedures arises from the small trapped fields in the superconducting magnets during cooling, which changes drastically the behavior of the material in the ordered phase. It is to be explained, nevertheless, why this happens. We suspect that a similar reason could underlie many of the negative magnetizations reported in similar materials,[16,46,47] as trapped fields in conventional SQUID magnetometers are usually negative.

It is worth mentioning that the application of moderate magnetic fields (i.e., 100 Oe) during the heating of the sample is not strong enough to reorient the magnetization on the sample in the direction of the magnetic field at some point of the heating curve. For 1000 Oe, the ZFC of the polycrystalline sample switches from negative to positive at around 25 K (Figure 3).

Hysteresis loops performed along the different directions are quite illustrative of the magnetic behavior of this system (Figure 7). Especially appealing is the result along the [010] direction and, moreover, the exotic initial magnetization curve (Figure 7c, green line).

First of all, it seems impossible to set to zero the magnetization of $(CH_3NH_3)[Ni(HCOO)_3]$ below 33 K along the [010] direction. In Figure 7c, it is seen that the initial magnetization curve starts from a negative value (due to a trapped field between −0.1 and 0 Oe), it switches to positive at 500 Oe, and, later on, the magnetization switches its sign at ∼±1.7 T, creating a hysteresis loop. However, the absolute value of M from which it jumps at 500 Oe to positive at the first run is the same as at the following runs, that is, it seems that this value corresponds to the fully magnetized sample. Why then at the first run it jumps from this state to positive at 500 Oe, but at the next rounds it jumps from practically the same state but at 1700 Oe and not at 500Oe? If the first jump from negative to positive at 500 Oe occurred from a value of M smaller than the value at next runs, one could understand why it also occurs at a smaller field, at 500 Oe. The question is why it jumps from the same value but at different fields.

DISCUSSION

The behavior of the first magnetization observed in Figure 7 confirms that the magnetic ground state determined through neutron diffraction experiments slightly changes when the applied magnetic field is above a critical value (500 Oe at 2 K). Therefore, an explanation for this effect needs to be found. In

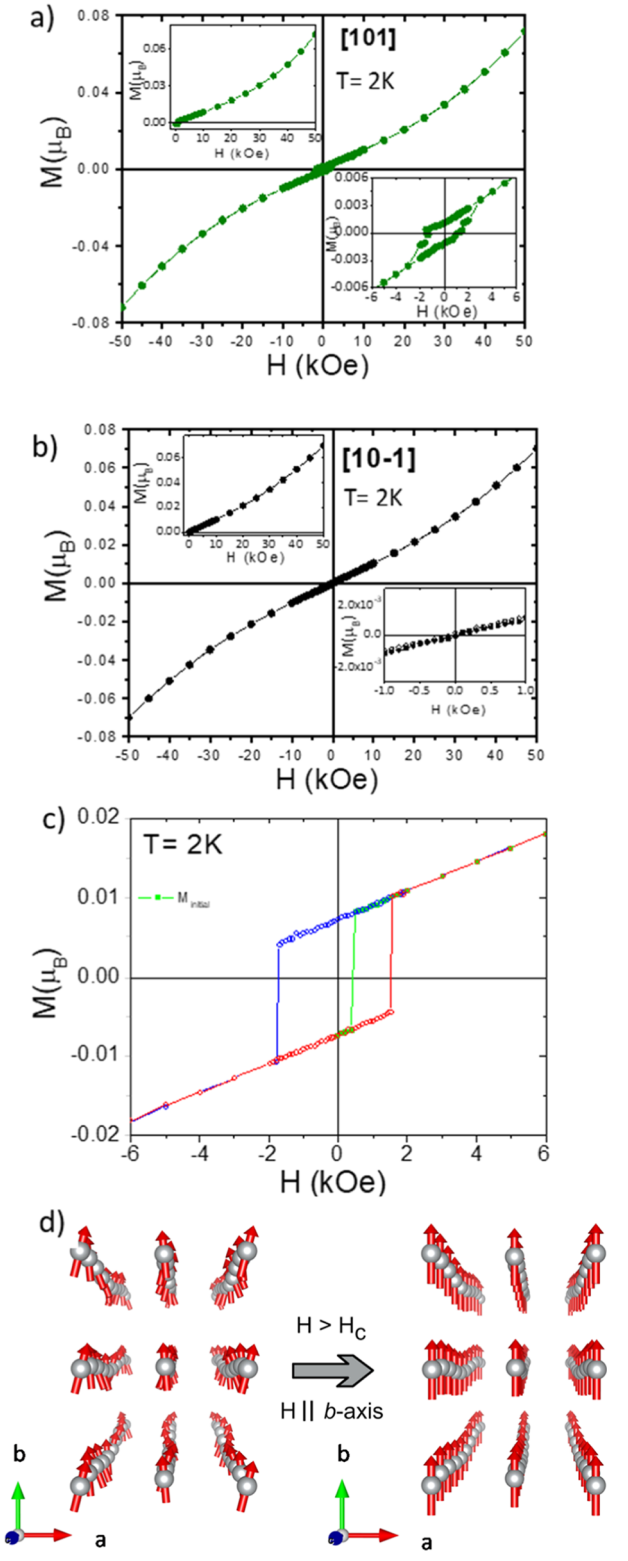

Figure 7. Isothermal magnetization of $(CH_3NH_3)[Ni(HCOO)_3]$ along (a) [101], (b) [10−1], and (c) [010] at 2 K. In (c), the initial magnetization at 0 Oe starts in negative values (green line), then it jumps to positive values at around 500 Oe, and, from that moment on, it follows a symmetrical hysteresis loop. (d) Effect of the suppression of proper magnetic modulations in the ferromagnetic component of the magnetic structure for fields larger than the coercive field, H_c (500 Oe at 2 K).

https://doi.org/10.1021/acs.jpcc.2c08364
J. Phys. Chem. C 2023, 127, 3330−3338

case the system was a classical spin canting system, as initially described, then the jump would always occur at the same applied magnetic field, as the energy to move the ferromagnetic component of the canting from negative to positive and vice versa is always the same. The fact that the first magnetization of the hysteresis loop follows a different path in subsequent magnetizations can be ascribed to the change in the magnetic ground state at higher fields.

Another interesting feature of this system is that it is not possible to set the magnetization to zero below 33 K. This can be explained by the influence that the magnetic field has over the sample: small magnetic fields align the ferromagnetic component along this applied field, decreasing the contribution of the magnetic domains. In a classic system with spin canting, the first magnetization goes to zero because when the temperature is lowered magnetic domains appear. These domains are randomly distributed, and as a result they cancel each other and the net magnetization is zero. This does not happen again after the first magnetization because the applied field forces the ferromagnetic moments to follow the direction of the applied field.

Another key in the analysis of $(CH_3NH_3)[Ni(HCOO)_3]$ is that the negative and positive branches of the magnetization curves are not completely specular (Figures 3, 5, and 6). From this, it can be concluded that the system cooled down at zero fields has also magnetic domains. However, these domains are not completely compensated as it occurs in classical systems; in this case, the ferromagnetic component can be modified with very weak magnetic fields; as can be seen from Figure 6, this feature precludes a complete domain compensation.

One must keep in mind that the ferromagnetic component of the incommensurate magnetic structure is not completely aligned along the *b* axis. There are small perpendicular components (based on the refined amplitudes of the proper magnetic modes, the main component is along the *a* axis) that provoke the appearance of incommensurability that can be seen as a "pendulum" of the magnetic moment on the *ab* plane (see Figures 2c or 7d). At zero field, the population of magnetic domains is unbalanced resulting in a non-negligible difference in magnetic susceptibility between the FC and ZFC measurements. However, when a small field is applied ($\ll$500 Oe), the magnetic domains tend to align with the external magnetic field, giving as a result a single domain system, where the susceptibility curve is symmetrical (Figure 5).

Therefore, as described above, the unbalance of the magnetic domains cannot be at the origin of the observed jump in the first magnetization at H_c (ca. 500 Oe). This jump must imply a change in the ground state of the magnetic structure. Since the effect is mainly observed when the field is applied in the *b* direction, this suggests that the ferromagnetic component observed at zero field remains in that direction in the underfield measurements for fields above 500 Oe. Once the critical field is overcome, the hysteresis loop presents a coercive field, H_c, of ca. 1.7 T, which is more than 3 times the critical field of the first magnetization. This coercive field is unbiased neither to positive nor to negative fields, which suggests that the zero-field-to-infield transition is not reversible. This irreversibility together with the relatively large coercive field suggests that the ferromagnetic component of the magnetic moments is better aligned with respect to the *b* axis, forming a modulated collinear magnetic structure. It deserves to be noted that when a magnetic material is under the influence of an external magnetic field, its global magnetic moment tends to align with the external magnetic field favoring collinear structures.

Most of the incommensurate magnetic structures have been observed in inorganic samples, for example, in the $Ca_3Co_{1.8}Fe_{0.2}O_6$ compound.[48] This compound at zero field orders magnetically in an incommensurate spin density wave structure with a Néel temperature of $\sim$ 20 K. However, the application of an external magnetic field of $\sim$2 T produces an incommensurate-to-commensurate magnetic phase transition. In this case, the incommensurate propagation vector $\mathbf{k}$ = [0, 0, and 1.0182(9)] evolves to a commensurate propagation vector $\mathbf{k}$ = (0, 0, 1), under an external magnetic field. Another example of spin reorientation involving the incommensurate magnetic structure is Li_2FeSnS_4.[49] The magnetic ordering in Li_2FeSnS_4 can be indexed with a propagation vector $\mathbf{k}$ = [0, 0, 0.546(1)], indicating an incommensurate AFM structure. A spin reorientation attributed to a spin flop phase is observed for magnetic fields of about 1.7 T at base temperature (1.5 K). A similar scenario could be observed on multiferroic manganite $RMnO_3$ (where *R* is a rare earth).[50−53]

To the best of our knowledge, this phenomenon has never been seen in pure organic magnets or in coordination polymer magnets, mainly because of the difficulty of obtaining complicated magnetic structures in these types of systems due to the small overlap between uncoupled electrons. To date, the only proper incommensurate magnetic structure reported is the compound discussed in the current manuscript. However, a similar phase transition was observed in the hybrid multiferroic compound $(NH_4)_2[FeCl_5{\cdot}(H_2O)]$, ammonium pentachloroaquaferrate(III), the only pentachloroaquaferrate-(III) that presents a magnetic incommensurate ground state.[54] This system at zero field presents a ground state described by the incommensurate propagation vector $\mathbf{k}$ = (0, 0, $\pm k_z$) with k_z = 0.23. Under an external magnetic field between 2.5 and 5 T, the magnetic structure evolves to a commensurate one, with $\mathbf{k}$ = (0, 0, $\pm k_z$) with k_z = 1/4. For magnetic fields above 5 T, a further spin orientation is observed, with a notable increase of intensity on top of the structural reflections, indicating a prevalence of a magnetic structure with propagation vector $\mathbf{k}$ = (0, 0, 0).

In order to achieve a magnetic collinear state, a transition from a magnetically incommensurate structure to a magnetically modulated collinear structure is needed. In other words, the proper magnetic modulations are suppressed leaving only active the improper modes, which are linked to the structure's displacements (see Figure 7d).

Similar behavior has been observed in inorganic and hybrid compounds with a magnetically incommensurate ground state. In these systems, the magnetic field generally induces a transition from the incommensurate phase to a magnetically collinear or commensurate phase.[48−54]

After the first magnetization, this structure remains invariant with only the expected flip of sense of the ferromagnetic component when the applied magnetic field changes from positive to negative overcoming the coercive field and vice versa. Given the soft ferromagnetic nature of this compound, once in the low-temperature magnetic collinear state, the system remains in this configuration even when the field is removed. The only way to return to the initial state is to heat the sample to the paramagnetic state and then cool it under zero field.

https://doi.org/10.1021/acs.jpcc.2c08364
J. Phys. Chem. C 2023, 127, 3330−3338

CONCLUSIONS

We have observed that the $(CH_3NH_3)[Ni(HCOO)_3]$ hybrid perovskite presents a series of uncommon features. The nuclear transition from the orthorhombic *Pnma* space group to the orthorhombic superspace group induced by the temperature is triggered by the changes in the hydrogen bond network. At lower temperatures, below Néel temperature, it presents both proper magnetic and nuclear incommensurability; this intricate magnetic structure occurs as a consequence of competing interactions. From the macroscopic magnetic measurements, we have observed that this compound shows several uncommon magnetic responses with nonzero susceptibility after ZFC procedures. This response is due to the noncompensation of the magnetic domains. The unbalance is caused by the small trapped fields in the superconducting magnets during the cooling of the sample. The magnetic field required to orient the ferromagnetic domains in the direction of the applied magnetic field is so weak that the competition between the trapped fields in the superconducting magnets and the magnetic field created by the sample itself precludes the compensation of magnetic domains.

When the hysteresis loops of this compound have been studied, surprisingly, the first magnetization follows a different pathway than subsequent magnetizations. However, although there is a change of sign in the magnetization, the curve continues smoothly, without showing a drastic change in the magnetization values in subsequent magnetizations. This effect is most visible when the field is applied in the *b* direction, the direction in which the ferromagnetic component is pointing. This involves the ferromagnetic component observed at zero field remaining mainly in the same direction after the switch above the critical field (500 Oe). Therefore, a drastic spin reorientation as in a spin flop system is discarded. After this first magnetization, the hysteresis loop exhibits a coercive field, which is more than 3 times the critical field of the initial magnetization. This coercive field is unbiased neither to positive nor to negative fields, which suggests that the zero-field-to-infield transition is not reversible. Furthermore, the reproducibility in the subsequent cycles rules out that it is an experimental effect (i.e., sample movement, etc.).

Considering the nuclear and magnetic structures obtained at zero field, the most plausible explanation is that the influence of the applied external field suppressed some of the active magnetic modes at zero field. The suppression of the proper magnetic modes slightly modifies the magnetization values, which explains why the magnetization cycles have no other feature than a change in sign at the critical field, but the resulting magnetic structure, a magnetically modulated collinear structure, is energetically more favorable, which explains the increase in the value of the coercive field.

AUTHOR INFORMATION

Corresponding Authors

Óscar Fabelo − *Institut Laue-Langevin, 38042 Grenoble, Cedex 9, France; Departamento de Física, Universidad de La Laguna, 38200 La Laguna, Tenerife, Spain*; Email: fabelo@ill.fr

Jorge Mira − *Departamento de Física Aplicada and iMATUS, Universidade de Santiago de Compostela, 15782 Santiago de Compostela, Spain*; orcid.org/0000-0002-6024-6294; Email: jorge.mira@usc.es

Authors

Breogán Pato-Doldán − *Department of Chemistry, Faculty of Sciences, Universidade da Coruña, 15071 A Coruña, Spain*

Laura Cañadillas-Delgado − *Institut Laue-Langevin, 38042 Grenoble, Cedex 9, France*

L. Claudia Gómez-Aguirre − *Department of Chemistry, Faculty of Sciences, Universidade da Coruña, 15071 A Coruña, Spain*

M. A. Señarís-Rodríguez − *Department of Chemistry, Faculty of Sciences, Universidade da Coruña, 15071 A Coruña, Spain*

Manuel Sánchez-Andújar − *Department of Chemistry, Faculty of Sciences, Universidade da Coruña, 15071 A Coruña, Spain*

Complete contact information is available at: https://pubs.acs.org/10.1021/acs.jpcc.2c08364

Author Contributions

⊥B.P.-D. and L.C.-D. contributed equally to this work.

Notes

The authors declare no competing financial interest.

ACKNOWLEDGMENTS

The authors thank financial support from the Ministerio de Economía y Competitividad MINECO and EU-FEDER (projects MAT2017-86453-R and PDC 2021-121076-I00). The authors are grateful to Dra. Ana Arauzo at Servicio de Medidas Físicas of the Universidad de Zaragoza for heat capacity data. O.F. acknowledges the Spanish Ministry of Universities (UNI/551/2021) and the European Union through the Funds Next Generation.

ABBREVIATIONS

ZFC, zero-field-cooled; FC, field-cooled; SQUID, superconducting quantum interference device

REFERENCES

(1) Yaghi, O. M.; O'Keeffe, M.; Ockwig, N. W.; Chae, H. K.; Eddaoudi, M.; Kim, J. Reticular Synthesis and the Design of New Materials. *Nature* **2003**, *423*, 705−714.

(2) Fletcher, A. J.; Thomas, K.; Rosseinsky, M. Flexibility in Metal-Organic Framework Materials: Impact on Sorption Properties. *J. Solid State Chem.* **2005**, *178*, 2491−2510.

(3) Allendorf, M. D.; Bauer, C. A.; Bhakta, R. K.; Houk, R. J. T. Luminescent Metal-Organic Frameworks. *Chem. Soc. Rev.* **2009**, *38*, 1330−1352.

(4) Guo, M.; Cai, H.-L.; Xiong, R.-G. Ferroelectric Metal Organic Framework (MOF). *Inorg. Chem. Commun.* **2010**, *13*, 1590−1598.

(5) Hang, T.; Zhang, W.; Ye, H.-Y.; Xiong, R.-G. Metal-Organic Complex Ferroelectrics. *Chem. Soc. Rev.* **2011**, *40*, 3577−3598.

(6) Zhang, W.; Xiong, R.-G. Ferroelectric Metal-Organic Frameworks. *Chem. Rev.* **2012**, *112*, 1163−1195.

(7) Cheetham, A. K.; Rao, C. N. R. There's Room in the Middle. *Science* **2007**, *318*, 58−59.

(8) Férey, G. Hybrid Porous Solids: Past, Present, Future. *Chem. Soc. Rev.* **2008**, *37*, 191−214.

(9) Liu, B.; Shang, R.; Hu, K.-L.; Wang, Z.-M.; Gao, S. A New Series of Chiral Metal Formate Frameworks of [HONH3][MII(HCOO)3] (M = Mn, Co, Ni, Zn, and Mg): Synthesis, Structures, and Properties. *Inorg. Chem.* **2012**, *51*, 13363−13372.

(10) Chen, S.; Shang, R.; Hu, K.-L.; Wang, Z.-M.; Gao, S. [NH2NH3][M(HCOO)3] (M = Mn2+, Zn2+, Co2+and Mg2+): structural phase transitions, prominent dielectric anomalies and negative thermal expansion, and magnetic ordering. *Inorg. Chem. Front.* **2014**, *1*, 83−98.

(11) Gómez-Aguirre, L. C.; Pato-Doldán, B.; Stroppa, A.; Yáñez-Vilar, S.; Bayarjargal, L.; Winkler, B.; Castro-García, S.; Mira, J.; Sánchez-Andújar, M.; Señarís-Rodríguez, M. A. Room-Temperature Polar Order in $[NH_4][Cd(HCOO)_3]$ - A Hybrid Inorganic−Organic Compound with a Unique Perovskite Architecture. *Inorg. Chem.* **2015**, *54*, 2109−2116.
(12) Pato-Doldán, B.; Gómez-Aguirre, L. C.; Bermúdez-García, J. M.; Sánchez-Andújar, M.; Fondado, A.; Mira, J.; Castro-García, S.; Señarís-Rodríguez, M. A. Coexistence of Magnetic and Electrical Order in the New Perovskite-like $(C_3N_2H_5)[Mn(HCOO)_3]$ Formate. *RSC Adv.* **2013**, *3*, 22404−22411.
(13) Tian, Y.; Stroppa, A.; Chai, Y.; Yan, L.; Wang, S.; Barone, P.; Picozzi, S.; Sun, Y. Cross Coupling between Electric and Magnetic Orders in a Multiferroic Metal-Organic Framework. *Sci. Rep.* **2014**, *4*, 6062.
(14) Jain, P.; Ramachandran, V.; Clark, R. J.; Zhou, H. D.; Toby, B. H.; Dalal, N. S.; Kroto, H. W.; Cheetham, A. K. Multiferroic Behavior Associated with an Order−Disorder Hydrogen Bonding Transition in Metal−Organic Frameworks (MOFs) with the Perovskite ABX3 Architecture. *J. Am. Chem. Soc.* **2009**, *131*, 13625−13627.
(15) Wang, Z.; Hu, K.; Gao, S.; Kobayashi, H.; Wang, B. Z.; Hu, K.; Gao, S.; Kobayashi, H. Formate-Based Magnetic Metal-Organic Frameworks Templated by Protonated Amines. *Adv. Mater.* **2010**, *22*, 1526−1533.
(16) Wang, X.-Y.; Gan, L.; Zhang, S.-W.; Gao, S. Perovskite-like Metal Formates with Weak Ferromagnetism and as Precursors to Amorphous Materials. *Inorg. Chem.* **2004**, *43*, 4615−4625.
(17) Baker, P. J.; Lancaster, T.; Franke, I.; Hayes, W.; Blundell, S. J.; Pratt, F. L.; Jain, P.; Wang, Z.-M.; Kurmoo, M. Muon Spin Relaxation Investigation of Magnetic Ordering in the Hybrid Organic-Inorganic Perovskites $[(CH_3)_2NH_2]M(HCOO)_3$, M = Ni, Co, Mn, Cu. *Phys. Rev. B: Condens. Matter Mater. Phys.* **2010**, *82*, 012407.
(18) Dzyaloshinsky, I. A. A thermodynamic theory of "weak" ferromagnetism of antiferromagnetics. *J. Phys. Chem. Solids* **1958**, *4*, 241−255.
(19) Sergienko, I. A.; Dagotto, E. Role of the Dzyaloshinskii-Moriya Interaction in Multiferroic Perovskites. *Phys. Rev. B: Condens. Matter Mater. Phys.* **2006**, *73*, 094434.
(20) Moriya, T. Theory of Magnetism of NiF2. *Phys. Rev.* **1960**, *117*, 635−647.
(21) Pato-Doldán, B.; Gómez-Aguirre, L. C.; Hansen, A. P.; Mira, J.; Castro-García, S.; Sánchez-Andújar, M.; Señarís-Rodríguez, M. A.; Zapf, V. S.; Singleton, J. Magnetic Transitions and Isotropic: Versus Anisotropic Magnetic Behaviour of $[CH_3NH_3][M(HCOO)_3]$ M = Mn^{2+}, Co^{2+}, Ni^{2+}, Cu^{2+} Metal-Organic Perovskites. *J. Mater. Chem. C* **2016**, *4*, 11164−11172.
(22) Gómez-Aguirre, L. C.; Pato-Doldán, B.; Mira, J.; Castro-García, S.; Señarís-Rodríguez, M. A.; Sánchez-Andújar, M.; Singleton, J.; Zapf, V. S. Magnetic Ordering-Induced Multiferroic Behavior in $[CH_3NH_3][Co(HCOO)_3]$ Metal-Organic Framework. *J. Am. Chem. Soc.* **2016**, *138*, 1122−1125.
(23) Mazzuca, L.; Cañadillas-Delgado, L.; Fabelo, O.; Rodríguez-Velamazán, J. A.; Luzón, J.; Vallcorba, O.; Simonet, V.; Colin, C. V.; Rodríguez-Carvajal, J. Microscopic Insights on the Multiferroic Perovskite-Like [CH3NH3][Co(COOH)3] Compound. *Chem.—Eur. J.* **2018**, *24*, 388−399.
(24) Canadillas-Delgado, L.; Mazzuca, L.; Fabelo, O.; Rodriguez-Velamazan, J. A.; Rodriguez-Carvajal, J. Incommensurate structures of the [CH3NH3][Co(COOH)3] compound. *IUCrJ* **2019**, *6*, 105−115.
(25) Néel, M. L. Propriétés Magnétiques Des Ferrites ; Ferrimagnétisme et Antiferromagnétisme. *Ann. Phys.* **1948**, *12*, 137−198.
(26) Zhao, J.-P.; Hu, B.-W.; Lloret, F.; Tao, J.; Yang, Q.; Zhang, X.-F.; Bu, X.-H. Magnetic Behavior Control in Niccolite Structural Metal Formate Frameworks [NH2(CH3)2][FeIIIMII(HCOO)6] (M = Fe, Mn, and Co) by Varying the Divalent Metal Ions. *Inorg. Chem.* **2010**, *49*, 10390−10399.
(27) Cañadillas-Delgado, L.; Fabelo, O.; Rodríguez-Velamazán, J. A.; Lemée-Cailleau, M. H.; Mason, S. A.; Pardo, E.; Lloret, F.; Zhao, J. P.; Bu, X. H.; Simonet, V.; et al. The Role of Order-Disorder Transitions in the Quest for Molecular Multiferroics: Structural and Magnetic Neutron Studies of a Mixed Valence Iron(II)-Iron(III) Formate Framework. *J. Am. Chem. Soc.* **2012**, *134*, 19772−19781.
(28) Nuttall, C. J.; Day, P. Magnetization of the Layer Compounds AFeIIFeIII(C2O4)3 (A = Organic Cation), in Low and High Magnetic Fields: Manifestation of Néel N and Q Type Ferrimagnetism in a Molecular Lattice. *Chem. Mater.* **1998**, *10*, 3050−3057.
(29) Mathonière, C.; Nuttall, C. J.; Carling, S. G.; Day, P. Ferrimagnetic Mixed-Valency and Mixed-Metal Tris(Oxalato)Iron-(III) Compounds: Synthesis, Structure, and Magnetism. *Inorg. Chem.* **1996**, *35*, 1201−1206.
(30) Carling, S. G.; Day, P.; Nuttall, C. J. Crystal and Magnetic Structures of AFeIIFeIII(C2O4)3 (A=organic Cation): Two-Dimensional Honeycomb Ferrimagnets. *Spectrochim. Acta, Part A* **2001**, *57*, 1971−1979.
(31) Kumar, A.; Yusuf, S. M.; Keller, L.; Yakhmi, J. V. Microscopic Understanding of Negative Magnetization in Cu, Mn, and Fe Based Prussian Blue Analogues. *Phys. Rev. Lett.* **2008**, *101*, 207206.
(32) Ohkoshi, S. I.; Arai, K. I.; Sato, Y.; Hashimoto, K. Humidity-Induced Magnetization and Magnetic Pole Inversion in a Cyano-Bridged Metal Assembly. *Nat. Mater.* **2004**, *3*, 857−861.
(33) Ohkoshi, S. I.; Hozumi, T.; Utsunomiya, M.; Abe, M.; Hashimoto, K. The Observation of Two Compensation Temperatures in a Cobalt-Manganese Hexacyanochromate. *Phys. B* **2003**, *329*−*333*, 691−692.
(34) Ohkoshi, S.; Iyoda, T.; Fujishima, A.; Hashimoto, K. Magnetic Properties of Mixed Ferro-Ferrimagnets Composed of Prussian Blue Analogs. *Phys. Rev. B: Condens. Matter Mater. Phys.* **1997**, *56*, 11642.
(35) Ohkoshi, S. I.; Abe, Y.; Fujishima, A.; Hashimoto, K. Design and Preparation of a Novel Magnet Exhibiting Two Compensation Temperatures Based on Molecular Field Theory. *Phys. Rev. Lett.* **1999**, *82*, 1285−1288.
(36) Ohkoshi, S. I.; Fujishima, A.; Hashimoto, K. Transparent and Colored Magnetic Thin Films: (FeIIxCrII1-x)1.5[CrIII(CN)6]. *J. Am. Chem. Soc.* **1998**, *120*, 5349−5350.
(37) Goodenough, J. B.; Nguyen, H. C. The Peculiar Ferromagnetism of $LaVO_3$. *C. R. Acad. Sci., Ser. IIb: Mec., Phys., Astron.* **1994**, *319*, 1285−1291.
(38) Ren, Y.; Palstra, D. I.; Khomskii, E.; Pellegrin, G. A.; Nugroho, A. A.; Menovsky, A. A.; Sawatzky, G. A. Temperature-induced magnetization reversal in a YVO3 single crystal. *Nature* **1998**, *396*, 441−444.
(39) Nguyen, H. C.; Goodenough, J. B. Magnetic Studies of Some Orthovanadates. *Phys. Rev. B: Condens. Matter Mater. Phys.* **1995**, *52*, 324−334.
(40) Rivas-Murias, B.; Rivadulla, F.; Sánchez-Andújar, M.; Castro-Couceiro, A.; Señarís-Rodríguez, M. A.; Rivas, J. Role of t2g versus eg Interactions in the Physical Properties of A2OBO3 (A = Mn, Fe). *Chem. Mater.* **2006**, *18*, 4547−4552.
(41) Menyuk, N.; Dwight, K.; Wickham, D. G. Magnetization Reversal and Asymmetry in Cobalt Vanadate (IV). *Phys. Rev. Lett.* **1960**, *4*, 119−120.
(42) Canãdillas-Delgado, L.; Mazzuca, L.; Fabelo, O.; Rodríguez-Carvajal, J.; Petricek, V. Experimental Evidence of the Coexistence of Proper Magnetic and Structural Incommensurability on the $[CH_3NH_3][Ni(COOH)_3]$ Compound. *Inorg. Chem.* **2020**, *59*, 17896−17905.
(43) Belik, A. a. Origin of Magnetization Reversal and Exchange Bias Phenomena in Solid Solutions of BiFeO3-BiMnO3: Intrinsic or Extrinsic? *Inorg. Chem.* **2013**, *52*, 2015−2021.
(44) Belik, A. a. Fresh Look at the Mystery of Magnetization Reversal in YVO3. *Inorg. Chem.* **2013**, *52*, 8529−8539.
(45) Kumar, N.; Sundaresan, A. On the Observation of Negative Magnetization under Zero-Field-Cooled Process. *Solid State Commun.* **2010**, *150*, 1162−1164.
(46) Mączka, M.; Gągor, A.; Macalik, B.; Pikul, A.; Ptak, M.; Hanuza, J. Order−Disorder Transition and Weak Ferromagnetism in the Perovskite Metal Formate Frameworks of $[(CH_3)_2NH_2][M-$

https://doi.org/10.1021/acs.jpcc.2c08364
J. Phys. Chem. C 2023, 127, 3330−3338

$(HCOO)_3$] and [$(CH_3)_2ND_2$][$M(HCOO)_3$] (M = Ni, Mn). *Inorg. Chem.* **2014**, *53*, 457−467.
(47) Hu, K.-L.; Kurmoo, M.; Wang, Z.; Gao, S. Metal-Organic Perovskites: Synthesis, Structures, and Magnetic Properties of [C(NH2)3][MII(HCOO)3] (M=Mn, Fe, Co, Ni, Cu, and Zn; C(NH2)3= Guanidinium). *Chem.—Eur. J.* **2009**, *15*, 12050.
(48) Yusuf, S. M.; Jain, A.; Keller, L. Field induced incommensurate-to-commensurate magnetic phase transition in Ca3Co1.8Fe0.2O6: a neutron diffraction study. *J. Phys.: Condens. Matter* **2013**, *25*, 146001.
(49) Brant, J. A.; dela Cruz, C.; Yao, J.; Douvalis, A. P.; Bakas, T.; Sorescu, M.; Aitken, J. A. Field-Induced Spin-Flop in Antiferromagnetic Semiconductors with Commensurate and Incommensurate Magnetic Structures: Li2FeGeS4 (LIGS) and Li2FeSnS4 (LITS). *Inorg. Chem.* **2014**, *53*, 12265−12274.
(50) Feyerherm, R.; Dudzik, E.; Aliouane, N.; Argyriou, D. N. Commensurate Dy magnetic ordering associated with incommensurate lattice distortion in multiferroicDyMnO3. *Phys. Rev. B: Condens. Matter Mater. Phys.* **2006**, *73*, 180401.
(51) Kenzelmann, M.; Harris, A. B.; Jonas, S.; Broholm, C.; Schefer, J.; Kim, S. B.; Zhang, C. L.; Cheong, S. W.; Vajk, O. P.; Lynn, J. W. Magnetic inversion symmetry breaking and ferroelectricity in TbMnO3. *Phys. Rev. Lett.* **2005**, *95*, 087206.
(52) Quezel, S.; Tcheou, F.; Rossat-Mignod, J.; Quezel, G.; Roudaut, E. Magnetic structure of the perovskite-like compound TbMnO3. *Physica B+C* **1977**, *86-88*, 916−918.
(53) Kajimoto, R.; Yoshizawa, H.; Shintani, H.; Kimura, T.; Tokura, Y. Magnetic Structure of $TbMnO_3$ by Neutron Diffraction. *Phys. Rev. B: Condens. Matter Mater. Phys.* **2004**, *70*, 012401.
(54) Rodríguez-Velamazán, J. A.; Fabelo, O.; Campo, J.; Millán, Á.; Rodríguez-Carvajal, J.; Chapon, L. C. Magnetic-Field-Induced Change of Magnetoelectric Coupling in the Hybrid Multiferroic $(ND_4)_2[FeCl_5 \cdot D_2O]$. *Phys. Rev. B: Condens. Matter Mater. Phys.* **2017**, *95*, 174439.

https://doi.org/10.1021/acs.jpcc.2c08364
J. Phys. Chem. C 2023, 127, 3330−3338